

# X-ray Dip Monitoring of XB 1916-053

T. Narita

*Department of Physics, College of the Holy Cross, Worcester, MA 01610*

J. E. Grindlay

*Harvard-Smithsonian Center for Astrophysics, Cambridge, MA 02138*

P. F. Bloser

*NASA/Goddard Space Flight Center, Greenbelt, MD 20771*

and

Y. Chou

*National Tsing Hua University, Taiwan*

## ABSTRACT

We report on the long term monitoring of X-ray dips from the ultracompact low-mass X-ray binary (LMXB) XB 1916-053. Roughly one-month interval observations were carried out with the *Rossi X-ray Timing Explorer* (RXTE) during 1996, during which the source varied between dim, hard states and more luminous, soft states. The dip spectra and dip lightcurves were compared against both the broadband luminosity and the derived mass accretion rate ( $\dot{M}$ ). The dips spectra could be fitted by an absorbed blackbody plus cut-off power law non-dip spectral model, with additional absorption ranging from 0 to  $> 100 \times 10^{22} \text{ cm}^{-2}$ . The amount of additional blackbody absorption was found to vary with the source luminosity. Our results are consistent with an obscuration of the inner disk region by a partially ionized outer disk. The size of the corona, derived from the dip ingress times, was found to be  $\sim 10^9 \text{ cm}$ . The corona size did not correlate with the coronal temperature, but seemed to increase when  $\dot{M}$  also increased. We discuss our findings in the context of an evaporated accretion disk corona model and an ADAF-type model.

*Subject headings:*

### 1. Introduction

The low-mass X-ray binary (LMXB) XB 1916-053 is the most compact X-ray binary which exhibit intensity reductions, or dips. It is generally accepted that the dips are due to the obscuration of the central object in a large inclination system by a bulge in the outer accretion disk (White & Swank 1982). XB 1916-053 was the first dipping source discovered, and has an X-ray period of  $\sim 3000$  seconds (Walter et al. 1982; White & Swank 1982). Since its discovery, XB

1916-053 has been the subject of numerous investigations. The dip spectra from *Exosat* (Smale et al. 1988) and *Ginga* (Smale et al. 1992; Yoshida et al. 1995) observations were best fit with a two component model. During the dips, one component was absorbed and the other component decreased in normalization. More recent observations with *ROSAT* (Morley et al. 1999), *ASCA* (Church et al. 1997), and *Beppo-SAX* (Church et al. 1998) found the deep dip spectra could be fit with a partially covered blackbody plus power-law model. In this model, the blackbody component is heavily ab-

sorbed but the power-law component is only partially absorbed. The normalization remains the same between dip and non-dip spectra.

The partial covering model implies an emission geometry where a compact blackbody is surrounded by an extended corona. This picture is also supported by *RXTE* observations of the non-dip emission from XB 1916-053 (Bloser et al. 2000a). However, there are other dipping LMXBs which clearly show different components. The eclipse spectrum of EXO 0748-676 shows a residual thermal emission lines from a low temperature corona while the harder component is heavily obscured (Bonnet-Bidaut et al. 2000). The dip spectrum from X 1658-298 shows the blackbody component with a smaller absorption than the Comptonizing component (Oosterbroek et al. 2001). It is puzzling that effects of the outer disk obscuration of the inner disk region can vary greatly, even in a relatively small range of inclination angles.

The purpose of this investigation is to study the relationship between mass accretion rate and spectral and timing behavior of the dips in XB 1916-053 using *RXTE* data. LMXBs, in general, show various spectral states or changes in luminosity. The change in luminosity has been typically used as a measure of the mass accretion on the compact object (Mitsuda et al. 1984). However, for atoll sources like XB 1916-053, it is also generally accepted that the motion within a color-color diagram (CCD) is a function of mass accretion (Hasinger & van der Klis 1989). Several recent observations show a strong correlation between atoll LMXB spectral parameters and motion within a CCD (Mendez et al. 1999; Bloser et al. 2000b; Gierlinski & Done 2002a; Munro et al. 2002). An earlier analysis of the non-dip spectral shape from XB 1916-053 also shows a correlated motion along its CCD which implies variation in  $\dot{M}$  (Bloser et al. 2000a).

## 2. Observations and Analysis

### 2.1. *RXTE* Observation and Data Reduction

XB 1916-053 was monitored by PCA and HEXTE instrument aboard *Rossi X-ray Timing Explorer* (*RXTE*) (Bradt et al. 1993) from 1996 February to 1996 October at roughly one month intervals. An additional 10 observations were per-

formed on consecutive days from 1996 May 14 to May 23. A detailed log of the observations can be found in Boirin et al. (2001). The analysis of the persistent emission, excluding dips and bursts, can be found in Bloser et al. (2000a).

The gain on the PCA detector has been changed on five occasions since mission start. Two of our observations were done during PCA Gain Epoch 1 and the remainder during Gain Epoch 3. Since each Epoch requires its own background models and response matrices, we could not confidently relate the spectral parameters from one Epoch to another (see Bloser et al. 2002a). Therefore, we excluded 1996 February 10 and 1996 March 13 data which were taken during PCA Gain Epoch 1 from further analysis.

For the remaining observations, we created two Good Time Intervals (GTI). The non-dip GTI excluded bursts, and primary and secondary dips. The primary dip ephemeris was taken from Chou et al. (2001). For each dip, we averaged the 2-30 keV PCA Standard-2 count rate to establish a baseline. The portion of the dip where the count rate was within 10% of the baseline was accumulated in the dip GTI. Due to Earth occultation coincident with the dips, we did not record any dip data from the 1996 May 5 observation. We also did not record any dip data from 1996 May 15 observation because the dips were not seen. Once the GTIs were defined, the non-dip and the deep dip data were reduced using the standard *RXTE* analysis tools in FTOOLS 5.1. The HEXTE spectral data were deadtime corrected and extracted from the standard archive mode data. The PCA spectral data were extracted from the Standard-2 data, which has 128 energy channels between 2 and 100 keV with 16 second time resolution. The PCA response matrices were generated with *pcarsp*. Spectra for each PCU and HEXTE cluster were reduced separately and combined within XSPEC v11.1.0.

### 2.2. Color-Color Diagram and Lightcurve

Bloser et al. (2000a) analyzed the non-dip emission by dividing the entire *RXTE* data into 70 segments of typical length  $\sim 1200$  s. By plotting each data segment as a point on a CCD, they found that XB 1916-053 traversed the lower and upper banana branches. Following Mendez et al. (1999), the CCD track was fit to a spline and each data

segment was parameterized with an  $S_a$  value on distance along the CCD location from the upper end of the CCD track for which  $S_a = 1.0$  was arbitrarily assigned. Here we are interested in the accretion rate, or the  $S_a$  parameter, for each observation date. In Figure 1, we replot the CCD using a different symbol for each observation date. The soft and hard colors are defined as the ratios of background-subtracted PCA count rates in the bands 3.5-6.4 keV and 2.0-3.5 keV, and 9.7-16.0 keV and 6.4-9.7 keV, respectively. In Table 1, we list an average  $S_a$  value for each observation date using the  $S_a$  values from the data segments (Bloser et al. 2000a).

Throughout the monitoring campaign, the ingress/egress times and the dip durations varied considerably. To quantitatively assess the relationship between spectral parameters and dip profile, we removed any bursts during or near dips and folded the Standard-2 data at the X-ray period of 3000.27 seconds (Chou et al. 2001) for each observation date. A typical background subtracted lightcurves in the energy ranges 2-30 keV and 2-6 keV are shown in Figure 2. In the observations when the additional dip blackbody absorption is required (see sec 2.2), the 2-6 keV intensity reduction was nearly 100% in the dips. In the broadband 2-30 keV folded lightcurve, the ingress and egress times were defined as the time to go from 10% below the non-dip count rate to 10% above the dip count rate. The dip duration was defined as the full-width at half-minimum. The dip profiles were usually not symmetric so we fitted the ingress and egress lightcurves separately with a polynomial, and considered the shorter of the two times as an upper limit measure of the corona size (see sec. 3.2). For clarity, we hereafter refer to the shorter of the two times as the ingress time. The results of dip profile fitting are listed in Table 1. The ingress and duration times were found to vary by a factor of three and factor of thirty respectively throughout our observations.

In the bottom two panels of Figure 3 and Figure 4 we show the dip duration and ingress time of each observation as a function of  $S_a$  and broadband luminosity (see sec. 2.3).

### 2.3. Spectral Fitting

For each observation date, single non-dip emission spectrum was extracted from the combined

PCA and HEXTE data sets. Based on the spectral fits to the archived Crab data, we used only the data between 2.5 to 20.0 keV from PCUs 0 & 1. A systematic error of 1% was added to all the channels using *grppha*. HEXTE data was selected from 20.0 keV to 50.0 keV. Bloser et al. (2000a) found that the non-dip emission could be fit with either a cut-off power law plus a blackbody model (CPL+BB) or a Comptonization plus a blackbody (CompTT+BB). Fitting with a disk blackbody plus a cut-off power law (Disk+CPL) was reported to give unreasonable fits. We too found the CPL+BB model gave good fits to the data, and could not fit the data with the Disk+CPL model. We also tried the CompTT+BB model. Although CompTT+BB gave acceptable fits, the error bars were very large, and we decided to use only the CPL+BB model for our analysis. Due to the PCA's insensitivity below 2.5 keV, the hydrogen column density  $N_H$  was not allowed to vary. Taking an average value from several previous X-ray observations (Smale et al. 1988, 1992; Yoshida et al. 1995; Morley et al. 1999), we fixed  $N_H = 2.0 \times 10^{21} \text{ cm}^{-2}$ . We list the best-fit parameters for the persistent emission in Table 2.

We extracted the dip PCA spectra in a similar manner as the non-dip spectra using the dip GTI. However, in many cases the HEXTE count rate was too low to effectively constrain the dip spectra. Since most of the spectral differences between non-dip and dip data occurred at  $< 20$  keV, we decided to use only the PCA data for the dip analysis.

X-ray dips are almost certainly due to obscuration of the central region by the outer accretion disk, and thus the non-dip emission model must also give acceptable fits to the dip emission with only the  $N_H$  allowed to vary. Initially, we tried a very crude model of increasing the absorption to the persistent emission model. This consistently gave unacceptable fits. Next, we allowed the absorption to vary independently between the BB and CPL components. The BB and CPL normalizations were fixed to the non-dip model. This gave acceptable fits to all data and the results are reported in Table 2.

We proceeded to examine the relationship between the dip spectra and the non-dip spectral shape (as parameterized by  $S_a$  on the CCD). There is growing evidence that the motion within

the CCD, and not necessarily luminosity, is the best indication of mass accretion  $\dot{M}$  in LMXBs (Hasinger & van der Klis 1989; van der Klis 2001; Gierlinski & Done 2002a). In the top two panels of Figure 3 we show the BB and CPL absorption parameters as a function of  $S_a$ . The BB absorption is modest ( $< 25 \times 10^{22} \text{ cm}^{-2}$ ) when  $S_a$  is smaller than 1.12 or greater than 1.40. In the intermediate range of  $S_a$ , the BB absorption fluctuates greatly. The CPL absorption is relatively constant at  $\sim 50 - 60 \times 10^{22} \text{ cm}^{-2}$ , with occasional increase to  $\sim 100 \times 10^{22} \text{ cm}^{-2}$ .

We also compared the dip spectra against the non-dip luminosity. In the top two panels of Figure 4 we show the BB and CPL absorption parameters with respect to the broadband 2–50 keV luminosity. The BB absorption is  $\sim 100 \times 10^{22} \text{ cm}^{-2}$  or greater at low luminosities. At  $\sim 0.5 \times 10^{37} \text{ ergs s}^{-1}$ , the additional BB absorption suddenly decreases to nearly zero and remains very small as the luminosity increases. Meanwhile, the CPL absorption again remains relatively constant regardless of the BB absorption. This variation in BB absorption is seen clearly when comparing the spectra from two observations. In Figure 5, we show an example of a large BB absorption dip spectrum versus a small BB absorption dip spectrum. It appears that the attenuation of the  $< 6$  keV photons is not nearly as large in the more luminous May 16th observation as in the Aug 16th observation. The best fit model for the May 16th data requires no additional BB absorption.

We checked to see whether our results were artifacts of the fitting procedure. First, we fixed the blackbody absorption to  $1000 \times 10^{22} \text{ cm}^{-2}$ , essentially eliminating the BB component, while letting the CPL absorption to vary. This gave unacceptable fits in all cases where the luminosity was greater than  $0.5 \times 10^{37} \text{ ergs s}^{-1}$ . Only May 20 and May 22 observations gave acceptable fits with no BB component. Second, we removed the restriction of fitting to the non-dip model and allowed all BB+CPL parameters to vary. In the majority of the data, the BB temperature, CPL photon index, and CPL cut-off energy was within  $1\sigma$  of the persistent model. More importantly, the BB absorption was still small for the bright observations and remained large for the dim observations.

### 3. Summary and Discussion

We present results of a long term *RXTE* monitoring of x-ray dips in XB 1916-053. The spectral changes during dips, and the dip ingress/egress and duration times were examined. The persistent emission is best fitted by blackbody and cut-off power law components. During the dips, the flux reduction is greatest in the 2-10 keV band, but extends up to 20 keV. The deep dip spectra are best described by the non-dip spectral model, usually with additional absorption for the blackbody and the cut-off power law components. On several observations, however, there is no increase in the blackbody absorption from non-dip to dip spectra. In one observation, the dips are not seen at all. This is in direct contrast to the *BeppoSAX* observation which found a strong absorption for the blackbody component. Our analysis of the 2-30 keV band lightcurves show time varying dips with complex structure.

#### 3.1. Dip Absorption

X-ray dips are most likely due to absorbing material in the outer accretion disk. One model for the dips proposed by Frank, King & Lasota (1987, hereafter FKL) considers the ballistic trajectory of the accreting material passing above and below the disk. The accretion stream circularizes close to the central source after shocking several times (Lubow & Shu 1975), and the ionization instability (Krolik et al. 1981) creates a bulge consisting of dense cool clouds among hotter lower-density medium. For the orbital period of XB 1916-053 and assuming a neutron star mass of  $1.4 M_\odot$ , FKL model predicts the radius of the circularizing ring to be  $r_h = 4.1 \times 10^9 \text{ cm}$ , with the vertical height of the bulge fixed at  $\sim 0.4r_h$ . The column density of an individual cloud is expected to be  $\sim 3 \times 10^{24} \text{ cm}^{-2}$ , consistent with our lower limits for the lower luminosity observations.

The small absorption of the blackbody component seen in XB 1916-053 may be due to partial ionization of the absorbing material. Partial ionization of the absorber have been proposed to explain the low energy excess seen in dips from several high mass X-ray binaries and black hole candidates in outburst (Marshall et al. 1993; Kuulkers et al. 1997). Although XB 1916-053 is a relatively dim source, the system is much more com-

compact and thus its outer disk could be ionized. At the circularization radius, the ionization parameter is  $\xi = L/nr_h^2$ , where  $L$  is the source luminosity and the  $n$  is the number density. We can estimate the number density as  $n = N_H/\Delta r$ , where  $\Delta r$  is the thickness of the absorbing material. With  $N_H \sim 100 \text{ cm}^{-2}$  and letting  $\Delta r \sim 0.1r_h$ , the number density is  $n \sim 2 \times 10^{15} \text{ cm}^{-3}$ . At the highest observed luminosity, the ionization parameter is  $\xi > 150 \text{ erg cm s}^{-1}$ . Near this value of  $\xi$  and at a density of  $n \sim 2 \times 10^{15} \text{ cm}^{-3}$ , the low-Z elements in the bulge are significantly ionized (Kallman & Bautista 2001).

Furthermore, the degree of ionization could be even higher in regions of low gas density in the bulge. The cold clouds, which initially condense out at the impact point, are expected to fall back toward the disk within  $\sim 0.5$  orbit (FKL). This may result in a lower density of gas near the top of the bulge, similar to the density variation observed from 4U 1822-37 (White & Holt 1982). Meanwhile, the near constant CPL absorption is likely due to the line of sight to the extended corona passing through both high and low density regions.

### 3.2. Physical extent of the corona

The CPL emission seen in many LMXBs are believed to originate in a hot optically thin gas nearby or surrounding the accretion disk. As the emission region or some fraction is occulted by the outer disk, we can use the ingress time to constrain the size of the emitting region or the absorber. If the angular extent of the absorber is larger than the emitting region, the size of the hot gas region is  $d = 2\pi\Delta Tr_h/P$ , where  $\Delta T$  is the ingress time and  $P$  is the period. On the other hand, if the absorber has a smaller angular extent than the emitting region, the equation above gives the size of the absorber. From the observed ingress times, the extent of either the CPL emission region or the absorber varies from  $d = 3.9 - 23.2 \times 10^8 \text{ cm}$ . To discern between the geometries, we examined the lightcurves and the spectra from all the observations. We find that in observations where the additional dip BB absorption is required, the 2-6 keV band dip intensity reduction is nearly 100%, implying that the CPL emission region is entirely covered by the absorber. We also find the dip CPL absorption to be nearly constant in all our observations, which suggests that there are no signifi-

cant differences in the angular sizes of the emitting region or the absorber from one observation to another. We therefore conclude that the ingress time constrains the size of the CPL emission region.

The possible mechanism for producing the hot gas can be divided into two broad categories. First possibility is the evaporation of the disk due to several forms of internal heating (Liang & Price 1977; Paczyński 1978) or external irradiation (Shakura & Sunyaev 1973), and the formation of an accretion disk corona (ADC). The extent of an ADC in hydrostatic equilibrium is governed by the temperature of the gas. The second possibility is an optically thin advection-dominated accretion flow (ADAF) type model. In such a case, the hot gas would reside within the optically thick accretion disk and the extent is likely a function of the mass accretion rate. With our observations, we can test both possibilities by comparing the CPL emission region size, as inferred from the ingress time, to temperature or mass accretion.

The extent of an ADC surrounding a compact object can be estimated from the relation  $R = 1 \times 10^{10} M/T_8$  where  $M$  is the mass of the neutron star in  $M_\odot$ , and the  $T$  is coronal temperature in  $10^8 \text{ K}$  (Begelman, McKee, & Shields 1983). Inferring the coronal temperature from the power-law cutoff energy (Haardt et al. 1993), we estimate the maximum radius of an optically thin and an optically thick corona at  $kT = 12 \text{ keV}$  to be  $1 \times 10^{10} \text{ cm}$  and  $4 \times 10^{10} \text{ cm}$ , respectively. According to FKL, a corona cannot extend beyond the circularization radius. Thus, in XB 1916-053 we expect the radius to increase as the temperature decreases, but become bound at the circularization radius ( $4.1 \times 10^9 \text{ cm}$ ) at the lowest temperatures. However, when we compare the CPL emission region size, as parameterized by the ingress time, to the CPL cut-off energy (Fig. 6), we find that the ingress time does not necessarily increase as the cut-off energy decreases. In fact, the smallest ingress time is associated with the lowest cut-off energy. We note however, that the size of the corona could be smaller if the heating is due mostly to accretion (Witt et al. 1997) or if an accretion disk wind develops at a much smaller radius (Murray et al. 1995).

Following Shapiro, Lightman & Eardley solution (1973), during period of low mass accretion in black hole systems, the inner part of the disk could

be replaced by a hot optically thin flow, such as an ADAF (Narayan & Yi 1994). When ADAF-type models are applied to black holes, the truncation radius, i.e. the extent of the hot gas, is highly uncertain but in all cases decreases with increasing  $\dot{M}$  (Abromowicz et al. 1995; Liu et al. 1999; Rozanska & Czerny 2000). The application of an ADAF model to a neutron star system is more difficult, however, due to the presence of a boundary layer (Narayan, Kato, & Honma 1997; Blandford & Begelman 1999; Medvedev & Narayan 2001). In our observations, the size of the CPL emission, as parameterized by the ingress time, does not become smaller with increasing  $S_a$ , corresponding to increasing  $\dot{M}$  (Fig. 3). The ingress times remain roughly constant for low values of  $S_a$ , and it actually increases to the largest value around  $S_a \sim 1.4$ . This may indicate that the observed accretion rate from XB 1916-053 is too large, and an ADAF-type flow in a neutron star system can only occur during periods of very low accretion (e.g. an island state) (Gierlinski & Done 2002b). Another possibility is that the luminous portion of the ADAF may be much smaller than the truncation radius (Medvedev & Narayan 2001), which will make the correlation between  $S_a$  and ingress time more uncertain. Finally, other observational evidence suggests that even if an ADAF like flow exists, its contribution to the CPL spectrum is minimal (Menou & McClintock 2002). Although it is interesting to note that an apparent decrease in the emission region size at  $S_a > 1.45$  (Fig. 3) coincides roughly with the sudden increase in the non-dip  $L_{BB}/L_{CPL}$  luminosity ratio (Bloser et al. 2000b). Such a scenario might be expected when the thermal photons from the boundary cools the ADAF-flow and causes it to collapse.

From our *RXTE* observations of XB 1916-053, we cannot say with certainty that the CPL emission originates in the ADC or the ADAF-type flow. We find that the extent of the hot gas can vary on days timescale, but the size does not correlate with temperature or mass accretion, as expected in simple ADC or ADAF models. What might be more likely is the coexistence of both types of hot plasma around the neutron star (Esin, McClintock, & Narayan 1997; Rozanska & Czerny 2000). In such a case, the truncation radius of the disk, and thus the extent of the ADAF-flow, may be better constrained by correlating the low

frequency quasi-periodic oscillations with the dip ingress times. This test may be better suited for black hole systems where the flow is not affected by the neutron star boundary layer.

TN acknowledges support from the College of the Holy Cross. PFB is a National Research Council Research Associate at NASA/Goddard Space Flight Center. This research has made use of data obtained through the High Energy Astrophysics Science Archive Research Center Online Service, provided by the NASA/Goddard Space Flight Center.

## REFERENCES

- Abramowicz, M.A., Chen, X., Kato, S., Lasota, J.-P., and Regev, O. 1995, *ApJ*, 438, L37
- Begelman, M.C., McKee, C.F., and Shields, G.A. 1983, *ApJ*, 271, 70
- Bloser, P.F., Grindlay, J.E., and Barret, D. 2000a, *ApJ*, 542, 989
- Bloser, P.F., Grindlay, J.E., Kaaret, P., Zhang, W., Smale, A.P., and Barret, D. 2000b, *ApJ*, 542, 1000
- Boirin, L., Barret, D., Olive, J.F., Grindlay, J.E., and Bloser, P.F. 2000, *A&A*, 361, 121
- Bonnet-Bidaud, J.M., Haberl, F., Ferrando, P., Bennie, P.J., and Kendziorra, E. 2000, *A&A*, 365, L282
- Blandford, R.D. and Begelman, M.C. 1999, *MNRAS*, 303, L1
- Bradt, H.V., Rothschild, R.E., and Swank, J.H. 1993, *A&AS*, 97, 355
- Chou, Y., Grindlay, J.E., and Bloser, P.F. 2001, *ApJ*, 549, 1135
- Church, M.J., Mitsuda, K., Dotani, T., and Bałucińska-Church, M. 1997, *ApJ*, 491, 388
- Church, M.J., Parmar, A.N., Bałucińska-Church, M., Oosterbroek, T., Dal Fiume, D., and Orlandini, M. 1998, *A&A*, 338, 556
- Esin, A.A., McClintock, J.E., and Narayan, R. 1997, *ApJ*, 489, 865

- Frank, J., King, A.R., and Lasota, J.-P. 1987, *Å*, 178, 137
- Gierlinski, M. and Done, C. 2002a, MNRAS, 331, L47
- Gierlinski, M. and Done, C. 2002b, MNRAS, 337, 1373
- Haardt, F., Done, C., Matt, G., and Fabian, A.C. 1993, ApJ, 411, L95
- Hasinger, G. and van der Klis, M. 1989, A&A, 225, 79
- Kallman, T. and Bautista, M. 2001, ApJ, 133, 221
- Krolik, J.H., McKee, C.F., Tarter, C.B. 1981, ApJ, 249, 422
- Kuulkers E., Wijnands, R., Belloni, T., Mendez, M., van der Klis, M., and van Paradijs, J. 1997, ApJ, 493, 753
- Liang, E.P.T., and Price, R.H. 1977, ApJ, 218, 247
- Liu, B.F., Yuan, W., Meyer, F., Meyer-Hofmeister, E., and Xie, G.Z. 1999, ApJ, 527, L17
- Lubow, S.H. and Shu, F.H., 1975, ApJ, 383, 198
- Marshall, F.E., Mushotzky, F.R., Petre, R., and Serlemitsos, P.J. 1993, ApJ, 419, 301
- Medvedev, M.V. and Narayan, R. 2001, ApJ, 554, 1255
- Mendez, M., van der Klis, M., Ford, E.C., Wijnands, R., and van Paradijs, J. 1999, ApJ, 511, L49
- Menou, K. and McClintock, J.E. 2002, ApJ, 557, 304
- Mitsuda, K., Inoure, H., Koyama, K. et al. 1984, PASJ, 36, 741
- Morley, R., Church, M.J., Smale, A.P., and Bałucińska-Church, M. 1999, MNRAS, 302, 593
- Muno, M., Remillard, R.A., and Chakrabarty, D. 2002, ApJ, 568, L35
- Murray, N., Chiang, J., Grossman, S.A., and Vorr, G.M. 1995, ApJ, 451, 498
- Narayan, R. and Yi, I. 1994, ApJ, 428, L13
- Narayan, R., Kato, S., and Honma, F. 1997, ApJ, 476, 49
- Oosterbroek, T., Parmar, A.N., Sidoli, L., in't Zand, J.J.M., and Heise, J. 2001, A&A, 376, 532
- Paczyński, B. 1977, Acta Astr., 28, 241
- Rozanska, A. and Czerny, B. 2000, A&A, 360, 1170
- Shakura, N.I. and Sunyaev, R.A. 1973, Astr. Ap., 24, 337
- Shapiro, S.L., Lightman, A.P., and Eardley, D.M. 1973, ApJ, 204, 187
- Smale, A.P., Mason, K.O., White, N.E., and Gottwald, M. 1988, MNRAS, 232, 647
- Smale, A.P., Mukai, K., Williams, O.R., Jones, M.H., and Corbet, R.H.D. 1992, ApJ, 400, 330
- van der Klis, M. ApJ, 561, 943
- Walter, F.M., Bowyer, S., Mason, K.O., Clark, J.T., Henry, J.P., Halpern, J. and Grindlay, J.E., 1982, ApJ, 253, L67
- White, N.E. and Swank, J.H. 1982, ApJ, 253, L61
- White, N.E. and Holt, S.S. 1982, ApJ, 257, 318
- Witt, J.J., Czerny, B., and Zycki, P.T. 1997, MNRAS, 286, 848
- Yoshida, K., Inoure, H., Mitsuda, K., Dotani, T., and Makino, F. 1995, PASJ, 47, 141

---

This 2-column preprint was prepared with the AAS L<sup>A</sup>T<sub>E</sub>X macros v5.0.

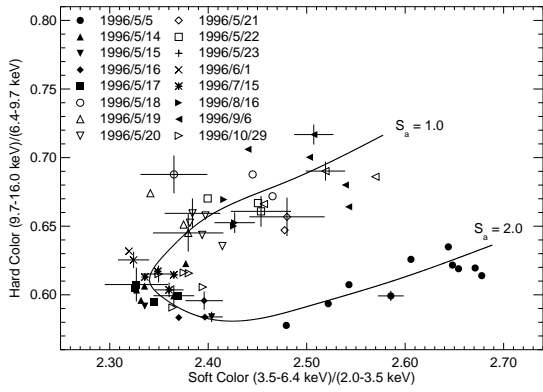


Fig. 1.— Color-color diagram of XB 1916-053. Each point represents a segment of the persistent emission with a typical length of 1200 s. Various symbols denote the different observation date. For clarity, only one set of error bars is displayed per date.



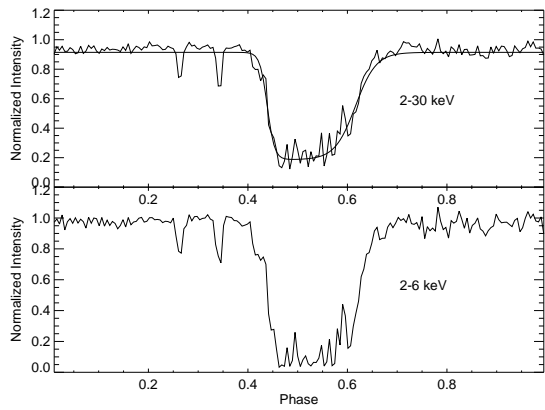


Fig. 2.— Folded lightcurves from May 14 1996 observation in the 2-30 keV and 2-6 keV energy bands. The 2-30 keV band lightcurve shows the best fit polynomial curve.

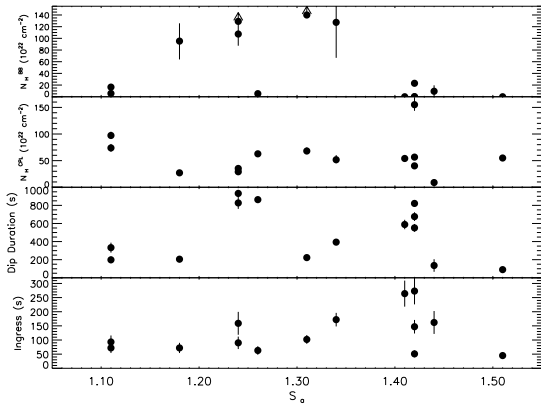


Fig. 3.— Variation of dip blackbody and cut-off power law absorption, and dip ingress and duration with accretion rate, parameterized by  $S_a$ . Error bars are  $1 \sigma$  for one interesting parameter.

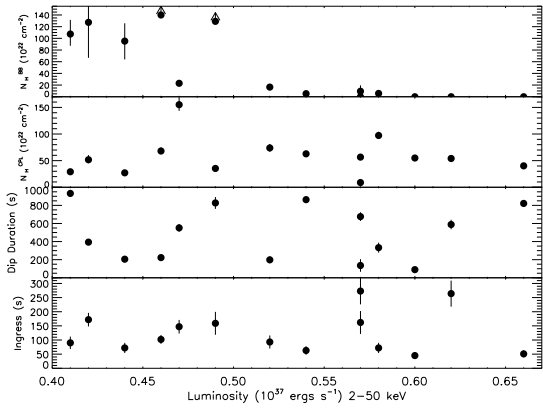


Fig. 4.— Variation of dip blackbody and cut-off power law absorptions, and dip ingress and duration with luminosity (2 – 50 keV). Error bars are  $1 \sigma$  for one interesting parameter.

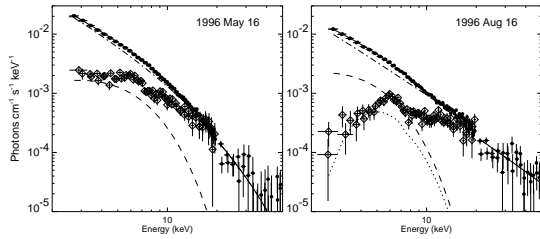


Fig. 5.— Examples of unfolded non-dip and dip spectra. The dash-dot line is the non-dip CPL model, and the dashed line is the non-dip BB model. On the left is the 1996 May 16 observation with little blackbody absorption during dips. On the right is the 1996 Aug 16 observation with large blackbody absorption. The dotted line in the Aug 16 plot shows the dip BB model. The dip CPL model is not shown for clarity.

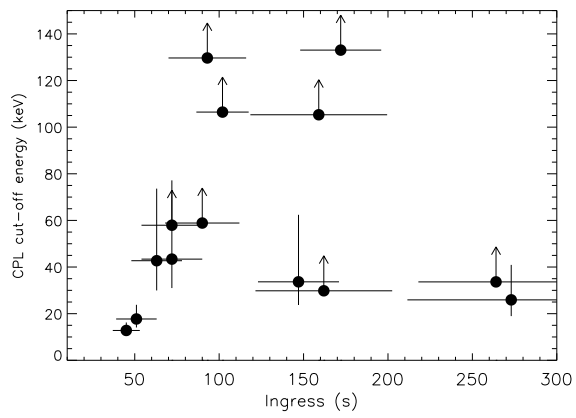


Fig. 6.— Comparison of CPL cut-off energy with ingress time.

TABLE 1  
DIP INGRESS/EGRESS AND DURATION.

Obs Date	$S_a$	$L^a$	Ingress (s)	Duration (s)
May 14 1996	1.42	0.47	$147 \pm 24$	$551 \pm 43$
May 16 1996	1.51	0.60	$45 \pm 8$	$90 \pm 13$
May 17 1996	1.44	0.57	$162 \pm 41$	$136 \pm 69$
May 18 1996	1.24	0.41	$90 \pm 22$	$932 \pm 38$
May 19 1996	1.34	0.42	$172 \pm 24$	$393 \pm 32$
May 20 1996	1.31	0.46	$102 \pm 16$	$222 \pm 28$
May 21 1996	1.18	0.44	$72 \pm 18$	$205 \pm 33$
May 22 1996	1.24	0.49	$159 \pm 41$	$826 \pm 65$
May 23 1996	1.41	0.62	$264 \pm 46$	$588 \pm 52$
June 1 1996	1.42	0.66	$51 \pm 12$	$821 \pm 28$
July 15 1996	1.26	0.54	$63 \pm 15$	$863 \pm 33$
Aug 16 1996	1.11	0.52	$93 \pm 23$	$198 \pm 37$
Sept 6 1996	1.42	0.57	$273 \pm 62$	$676 \pm 48$
Oct 29 1996	1.11	0.58	$72 \pm 18$	$333 \pm 55$

NOTE.—Errors are  $1\sigma$  for one interesting parameter.

<sup>a</sup>Total 2-50 keV luminosity, times  $10^{37}$  ergs  $s^{-1}$  for a distance of 9.3 kpc.

TABLE 2  
PERSISTENT EMISSION AND DIP SPECTRAL FITS OF XB 1916-053.

Obs Date	$S_a$	$kT_{BB}^a$	Persistent Emission			Dip Emission			$\chi_\nu^2$
			$\alpha^b$	$E_c^c$	$L^d$	$N_H(BB)^e$	$N_H(CPL)^f$		
May 14 1996	1.42	$1.48 \pm 0.06$	$1.89 \pm 0.09$	$33.66^{+28.74}_{-9.05}$	0.47	$23.1 \pm 3.1$	$155.1 \pm 11.4$	0.89	
May 16 1996	1.51	$1.70 \pm 0.06$	$1.64 \pm 0.08$	$12.80^{+3.42}_{-2.22}$	0.60	$0 + 0.220$	$55.0 \pm 5.3$	1.07	
May 17 1996	1.44	$1.58 \pm 0.05$	$1.99 \pm 0.10$	$> 29.8$	0.57	$9.41 \pm 9.50$	$8.85 \pm 1.7$	0.94	
May 18 1996	1.24	$1.39 \pm 0.05$	$1.89 \pm 0.03$	$> 58.9$	0.41	$107.5 \pm 22.5$	$29.1 \pm 1.5$	1.12	
May 19 1996	1.34	$1.50 \pm 0.11$	$1.83 \pm 0.21$	$> 133.0$	0.42	$> 66$	$51.7 \pm 5.5$	0.61	
May 20 1996	1.31	$1.47 \pm 0.04$	$1.96 \pm 0.02$	$> 106.5$	0.46	$> 140$	$68.1 \pm 5.8$	0.77	
May 21 1996	1.18	$1.45 \pm 0.05$	$1.92 \pm 0.10$	$> 57.9$	0.44	$95.3 \pm 31.0$	$27.1 \pm 3.4$	0.43	
May 22 1996	1.24	$1.45 \pm 0.04$	$1.94 \pm 0.06$	$> 105.3$	0.49	$> 129$	$35.3 \pm 1.1$	0.86	
May 23 1996	1.41	$1.60 \pm 0.05$	$2.05 \pm 0.13$	$> 33.6$	0.62	$0 + 0.5$	$54.1 \pm 3.6$	1.29	
June 1 1996	1.42	$1.56 \pm 0.02$	$1.74 \pm 0.09$	$17.72^{+6.09}_{-3.65}$	0.66	$0 + 0.2$	$40.2 \pm 2.1$	1.40	
July 15 1996	1.26	$1.44 \pm 0.06$	$1.82 \pm 0.08$	$42.71^{+30.94}_{-12.76}$	0.54	$5.27 \pm 1.0$	$62.8 \pm 2.7$	1.07	
Aug 16 1996	1.11	$1.34 \pm 0.03$	$1.81 \pm 0.02$	$> 129.7$	0.52	$16.50 \pm 2.0$	$73.9 \pm 6.2$	0.75	
Sept 6 1996	1.42	$1.64 \pm 0.06$	$1.87 \pm 0.11$	$25.92^{+15.01}_{-6.97}$	0.57	$0 + 0.10$	$56.6 \pm 2.6$	1.02	
Oct 29 1996	1.11	$1.40 \pm 0.06$	$1.74 \pm 0.08$	$43.40^{+33.77}_{-12.42}$	0.58	$5.66 \pm 1.2$	$97.3 \pm 6.3$	0.67	

NOTE.—For all persistent emission fits  $N_H$  is frozen at  $0.2 \times 10^{22} \text{ cm}^{-2}$ . Errors are  $1\sigma$  for one interesting parameter.

<sup>a</sup>Blackbody temperature (keV).

<sup>b</sup>Cut-off power law photon index.

<sup>c</sup>Cut-off power law cut-off energy (keV).

<sup>d</sup>Total 2-50 keV luminosity, times  $10^{37} \text{ ergs s}^{-1}$  for a distance of 9.3 kpc.

<sup>e</sup> $N_H$ ,  $\times 10^{22} \text{ cm}^{-2}$ , for blackbody component.

<sup>f</sup> $N_H$ ,  $\times 10^{22} \text{ cm}^{-2}$ , for cut-off power law component.